Molecular Pharmacology Fast Forward. Published on July 31, 2012 as doi: 10.1124/mol.112.080820
This article has been copyedited and formatted. The final version may differ from this version.

MOL #80820

**P6981, an arylstibonic acid, is a novel low nanomolar inhibitor of CREB binding to DNA**

Jianfei Zhao, Jason R. Stagno, Lyuba Varticovski, Eric Nimako, Vikas Rishi, Kathy McKinnon, Rhone Akee, Robert H. Shoemaker, Xinhua Ji, and Charles Vinson

*Laboratory of Metabolism (J.Z., E.N., V.R., C.V.), National Cancer Institute, Bethesda, MD 20892; Macromolecular Crystallography Laboratory (J.R.S., X.J.), National Cancer Institute, Frederick, MD 21702; Laboratory of Receptor Biology and Gene Expression (L.V., K.M.), Vaccine Branch, National Cancer Institute, Bethesda, MD 20892; Natural Products Support Group (R.A.), SAIC-Frederick, Frederick, MD 21702; and Developmental Therapeutics Program (R.H.S.), Frederick National Laboratory for Cancer Research, Frederick, MD 21702*

Molecular Pharmacology Fast Forward. Published on July 31, 2012 as DOI: 10.1124/mol.112.080820
This article has not been copyedited and formatted. The final version may differ from this version.

MOL #80820

Running title: P6981 inhibits DNA binding of B-ZIP at low nM concentrations

Corresponding author: Charles Vinson

Address: Building 37, Room 3128, 37 Convent DR, Laboratory of Metabolism, Center for Cancer Research, National Cancer Institute, Bethesda, MD 20892, USA.

Tel.: (301) 496-8753

Fax: (301) 496-8419

Email: vinsonc@mail.nih.gov

Text Pages: 28

References: 51

Abstract: 234 words

Introduction: 433 words

Discussion: 918 words

Nonstandard abbreviations: B-ZIP, basic leucine zipper; B-HLH-ZIP, basic helix-loop-helix leucine zipper; BR, basic region; LZ, leucine zipper; EMSA, electrophoretic mobility shift assay; C/EBP, CCAAT/enhancer binding protein; CREB, cyclic AMP response element binding protein; VBP, vitellogenin gene binding protein; Mitf, microphthalamia-associated transcription factor; USF, upstream stimulating factor; GFP, green fluorescent protein; GR, glucocorticoid receptor; A-ZIP, acidic leucine zipper; EWS, Ewing's Sarcoma protein; ATF, activating transcription factor; AP-1, activator protein; Bcr, breakpoint cluster region; Abl, Abelson murine leukemia oncogene.

Molecular Pharmacology Fast Forward. Published on July 31, 2012 as DOI: 10.1124/mol.112.080820
This article has not been copyedited and formatted. The final version may differ from this version.



**ABSTRACT**

Several B-ZIP transcription factors have been implicated in cancer, substance abuse, and other pathological conditions. We previously identified arylstibonic acids that bind to B-ZIP proteins and inhibit their interaction with DNA. In this study, we used EMSA to analyze 46 arylstibonic acids for their activity to disrupt the DNA binding of three B-ZIP (C/EBPα, CREB and VBP) and two B-HLH-ZIP (USF and Mitf) proteins. 25 arylstibonic acids showed activity at micromolar concentrations. The most active compound, P6981, had half-maximal inhibition at ~5 nM for CREB. Circular dichroism thermal denaturation studies indicated that P6981 binds both the B-ZIP domain and the leucine zipper. The crystal structure of an arylstibonic acid, NSC13778, bound to the VBP leucine zipper identified electrostatic interactions between both the stibonic and carboxylic acid groups of NSC13778 and arginine side-chains of VBP that is also involved in interhelical salt bridges in the leucine zipper. P6981 induced GFP-B-ZIP chimeric proteins to partially localize to the cytoplasm, demonstrating that it is active in cells. P6981 inhibited the growth of a patient-derived clear cell sarcoma cell line, whose oncogenic potential is driven by a chimeric protein EWS-ATF1 which contains the DNA binding domain of ATF1, a B-ZIP protein. NSC13778 inhibited the growth of xenografted clear cell sarcoma and no toxicity was observed. These experiments suggest that antimony containing arylstibonic acids are promising leads for suppression of DNA binding activities of B-ZIP and B-HLH-ZIP transcription factors.

Molecular Pharmacology Fast Forward. Published on July 31, 2012 as DOI: 10.1124/mol.112.080820
This article has not been copyedited and formatted. The final version may differ from this version.



**Introduction**

B-ZIP and B-HLH-ZIP proteins are two structurally related families of dimeric transcription factors that contain an α-helical basic region (BR) critical for DNA binding, and a leucine zipper (LZ) domain essential for dimerization (Vinson et al., 1989; Vinson and Garcia, 1992; Massari and Murre, 2000; Vinson et al., 2002). Members of these two protein families are required in a wide range of biological processes, such as immune response, metabolism, cell differentiation and proliferation (Corre and Galibert, 2005; Mayr and Montminy, 2001; Nerlov, 2008; Widlund and Fisher, 2003; Xiao et al., 2010). Elevated DNA-binding activities of some B-ZIP and B-HLH-ZIP proteins, such as CREB and Mitf, through dysregulation of upstream signaling pathways, have been implicated in human cancers, substance abuse, and other pathologies (Bonci and Carlezon, 2005; Giuliano et al., 2010; Shankar et al., 2005; Shukla et al., 2009). The inhibition of their DNA binding activities by dominant negatives has been shown to prevent and reverse some of these pathological states (Gerdes et al., 2006; Oh et al., 2007; Rozenberg et al., 2009; Walton et al., 1992; Xie et al., 1997).

The results obtained by genetically inhibiting the DNA binding of unique families of B-ZIP proteins suggest that they are potentially attractive drug targets. However, B-ZIP proteins are devoid of a catalytic pocket, complicating the identification of small molecules that inhibit B-ZIP|DNA interactions. A small molecule that disrupts the B-ZIP protein|DNA complex has recently been identified from a screen of the National Cancer Institute Diversity Library that contains 1,990 small molecules (Rishi et al., 2005). NSC13778, an arylstibonic acid, binds to and stabilizes the C/EBPα dimer, and inhibits the binding of C/EBPα to DNA. A subsequent study using 14 additional arylstibonic acid derivatives of NSC13778 identified that NSC13746 inhibits the DNA binding of C/EBPβ at sub-micromolar concentrations *in vitro* and specifically suppresses the transcriptional activation of B-ZIP proteins in a luciferase reporter assay (Rishi et al., 2010). NSC13746 also decreases the proliferation of a clear cell sarcoma cell line, CCS-1, which expresses EWS-ATF1 chimeric protein containing the B-ZIP domain of ATF1, a CREB family member (Rishi et al., 2010). These results suggest that arylstibonic acids could be

Molecular Pharmacology Fast Forward. Published on July 31, 2012 as DOI: 10.1124/mol.112.080820
This article has not been copyedited and formatted. The final version may differ from this version.



promising lead compounds to treat cancers or other diseases driven by constitutively activated B-ZIP proteins.

In this study, 46 arylstibonic acids, all derivatives of NSC13778 and NSC13746, were screened using EMSA for their inhibitory activities against the DNA binding of three B-ZIP (CREB, C/EBPα, and VBP) and two B-HLH-ZIP proteins (USF and Mitf). P6981, the most potent inhibitor identified, was further characterized by assessing the mechanism of inhibition, and by evaluating its effect on tumor cell proliferation.



## Materials and Methods

**Arylstibonic acid library.** The 46-member arylstibonic acid compound library was provided by the Developmental Therapeutics Program, Frederick National Laboratory for Cancer Research. The arylstibonic acids were obtained as powders and dissolved in 50 mM $NH_4OAc$, pH 9.0, aliquoted, and stored at -20 °C. 17 compounds had very low solubility in the experimental conditions, or they contained insoluble impurities.

12 arylstibonic acids used in this study have been previously characterized for their inhibitory activities against AP1, VBP, C/EBPα, C/EBPβ, and CREB (Rishi et al., 2010). They were included in this study as controls, and also to investigate their inhibitory activities against Mitf and USF. The results from the two studies are mostly consistent, with the exception of NSC13740 and NSC13743, which, in the previous study, were shown to be active at 10 μM and 1 μM, respectively, but were inactive here (data not shown). The discrepancy likely resulted from variable solubility in the experimental conditions, or from variable purity of the samples used in the two studies. However, the most active compounds identified in this and previous study, P6981 and NSC13746, were purified to ≥95% purity (Supplemental Fig. 1).

**Proteins.** Two synthesized VBP-LZs, VBP47 and VBP39 (Biopeptide), were kindly provided by David Waugh, National Cancer Institute-Frederick. The amino acid sequence corresponding to the VBP-LZ is underlined.

Molecular Pharmacology Fast Forward. Published on July 31, 2012 as DOI: 10.1124/mol.112.080820
This article has not been copyedited and formatted. The final version may differ from this version.



VBP47: RDPDLEIRAAFLEKENTALRTEVAELRKEVGRCKNIVSKYETRYGPL

VBP39: RDPDLEIRAAFLEKENTALRTEVAELRKEVGRCKNIVSK

The H2A-H2B chimera protein was a gift from Yawen Bai, National Cancer Institute. All other proteins used in this study have been previously described, including C/EBPα (Krylov et al., 1995), C/EBPβ (Rishi et al., 2005), CREB (Ahn et al., 1998), CREB-LZ (Ahn et al., 1998), VBP (Moll et al., 2000), VBP-LZ (Moll et al., 2000), Mitf (Rishi et al., 2004), and USF (Rishi et al., 2004). The recombinant proteins were overexpressed in the *E. coli* BL21 (LysE) strain and purified as described previously (Krylov et al., 1995; Olive et al., 1997; Rishi et al., 2010).

**DNA oligonucleotide.** The DNA oligonucleotides were PAGE purified (Sigma-Aldrich). The sense strand sequences of the 28-mer oligonucleotides for the EMSAs are:

CRE: GTCAGTCAGATGACGTCATATCGGTCAG

C/EBP: GTCAGTCAGATTGCGCAATATCGGTCAG

VBP: GTCAGTCAGATTACGTAATATCGGTCAG

E-box: GTCAGTCAGGCCACGTGAGATCGGTCAG

The consensus binding sites for the B-ZIP and B-HLH-ZIP proteins are underlined. The sense strand was end-labeled with $\gamma$-$^{32}$P ATP (specific activity 5000 Ci/mmol, MP Biomedicals) using T4 polynucleotide kinase (New England Biolabs), and was purified by the ProbeQuant G-50 micro column (GE Healthcare). The double-stranded DNA probes were generated by annealing the labeled sense strand and unlabeled anti-sense strand.

**Cell lines.** The suspension cells K562, a BCR/ABL transformed cell line, was obtained from ATCC. The clear cell sarcoma of soft tissue cell line, SU-CCS-1, bearing a transforming EWS/ATF-1 translocation, was a gift from Alan Epstein, University of Southern California. Both cell lines were maintained in RPMI media supplemented with 10% FCS (Hyclone) and glutamine (Invitrogen).

**Electrophoretic mobility shift assay (EMSA)**. EMSA was carried out to test the inhibitory effects of the arylstibonic acids on DNA binding of B-ZIP and B-HLH-ZIP proteins. Protein stock solutions (5 μM dimer) were heated at 65 °C for 15 min in the presence of 1 mM DTT, followed by

Molecular Pharmacology Fast Forward. Published on July 31, 2012 as DOI: 10.1124/mol.112.080820
This article has not been copyedited and formatted. The final version may differ from this version.



cooling at room temperature for 5 min. Protein dimers were then added to the gel shift reaction buffer (0.5 mg/ml BSA, 10% glycerol, 2.5 mM DTT, 12.5 mM $K_2HPO_4$-$KH_2PO_4$, pH 7.4, 0.25 mM EDTA) in the presence or absence of the arylstibonic acids, and the mixture was incubated at 37 °C for 5 min. 7 pM $^{32}$P-labeled 28-mer double-stranded oligonucleotide was then added, and the final volume of the reaction was adjusted to 20 µl. The reaction was incubated at 37 °C for 15 min, followed by cooling at room temperature for 5 min before being loaded to a 7.5% polyacrylamide gel. The protein|DNA complexes were separated by electrophoresis at 150 V for 90 min in 1×TBE buffer (25 mM Tris-boric acid, 0.5 mM EDTA). The gel was dried, and the autoradiograph was generated by exposure to a Kodak MR X-ray film or by phosphor imaging (GE Healthcare).

EMSAs with the nuclear extracts were conducted similarly. Briefly, 5 µg mouse liver nuclear extracts, purified as previously described (Rishi et al., 2010), were added to the gel shift reaction buffer (10 mM HEPES, pH 8.0, 6% glycerol, 80 mM KCl, 0.05 mM EDTA, 1 mM $MgCl_2$ and 1 mM DTT) in the presence or absence of the arylstibonic acids, and the mixture was incubated at 37 °C for 15 min, followed by cooling at room temperature for 5 min. 7 pM $^{32}$P-labeled DNA probes were added, and the reaction was incubated at 37 °C for 15 min. After incubation at room temperature for 5 min, the reaction was resolved by a 6% polyacrylamide gel at 150 V for 90 min in the 1×TBE buffer. The reaction also contained 1 µg poly (dI·dC) to prevent non-specific protein|DNA interactions.

**Inhibition potency determination.** The half-maximal inhibition concentrations ($IC_{50}$) were estimated by determining the arylstibonic acid concentrations at which equal intensities of the bands corresponding to the protein|DNA complex and the free DNA were produced on the EMSA gel.

**Circular dichroism (CD) spectroscopy.** CD spectroscopy was performed using a Jasco J-720 spectropolarimeter. All samples were prepared in the CD buffer containing 12.5 mM $K_2HPO_4$-$KH_2PO_4$ (pH 7.4), 150 mM KCl, 0.25 mM EDTA, and 1 mM DTT, except that KCl concentrations were varied from 15 to 2,000 mM in the salt-dependent experiments. Prior to CD spectroscopy measurement, the proteins were heated in the CD buffer at 65 °C for 15 min, followed by cooling at room temperature for 5 min. Arylstibonic acid was then added, and the reaction was incubated at 37 °C for 30 min before CD

Molecular Pharmacology Fast Forward. Published on July 31, 2012 as DOI: 10.1124/mol.112.080820
This article has not been copyedited and formatted. The final version may differ from this version.



analyses. For the thermal stability studies, the samples were heated from 6 to 85 °C with a heating rate of 1 °C/min. Changes in ellipticity ($\theta$, mdeg) for the proteins were recorded at 222 nm by the spectropolarimeter. The thermal denaturation curves were fitted as previously described (Krylov et al., 1994) according to equation 2:

$$[\theta] = (N - D) \times \left(1 - \frac{T}{INTR}\right) \times \left(1 + \frac{1 - \sqrt{8e^{\Delta Hm / R\left(\frac{1}{Tm+273} - \frac{1}{T+273}\right)} + 1}}{4 \times e^{\Delta Hm / R\left(\frac{1}{Tm+273} - \frac{1}{T+273}\right)}}\right) + D \qquad (1)$$

where $T$ is temperature (°C), $N$ and $D$ are the values of $\theta_{222}$, at 0 °C, of monomer and dimer, respectively, *INTR* is the temperature at which linear temperature-dependencies of dimer and monomer intercept, $T_m$ is the midpoint of the thermal denaturation (°C), $\Delta H_m$ is the enthalpy change (cal/mol) at $T_m$, and $R$ is the universal gas constant (2.0 cal·°C $^{-1}$·mol$^{-1}$).

**VBP39-NSC13778 complex formation, crystallization, and structure solution.** 1.25 μmol of NSC13778 were dissolved in 10 ml of 25 mM HEPES, pH 7.5, 50 mM KCl, and 0.25 mM EDTA. 1 μmol of the synthetic VBP39 peptide was added, and the solution was incubated in a 65 °C water bath for 15 min, followed by overnight rocking at room temperature. The peptide-inhibitor complex was concentrated to a protein concentration of 10 mg/ml on the following day. Crystallization was carried out at room temperature using sitting-drop vapor diffusion. Very fine needle-like crystals of the complex were grown from crystallization buffer containing 0.2 M ammonium phosphate, 20% PEG 3350, and 3% trimethylamine N-oxide, and cryoprotected in crystallization buffer supplemented with 20% ethylene glycol. X-ray diffraction data were collected at Stanford Synchrotron Radiation Lightsource (SSRL) beamline 7-1 and processed with XDS (Kabsch, 2010) to 3.3-Å resolution. The structure was solved by molecular replacement using PDB entry 1CE9 (Lu et al., 1999) as a search model, and refined using PHENIX (Adams et al., 2002) with non-crystallographic symmetry restraints applied to backbone atoms. The final model was validated using MolProbity (Chen et al., 2010). Structural illustrations were generated using PyMol (Delano Scientific). Data collection and refinement statistics are summarized in Supplemental Table 3.

Molecular Pharmacology Fast Forward. Published on July 31, 2012 as DOI: 10.1124/mol.112.080820
This article has not been copyedited and formatted. The final version may differ from this version.



**Transfection and confocal microscopy.** Murine NIH-3T3 cells were maintained in the DMEM media with 4.5 g/L D-glucose and 110 mg/L sodium pyruvate (Invitrogen), supplemented with 10% bovine calf serum and 1 mg/ml penicillin/streptomycin in a 5% $CO_2$ incubator at 37 °C. $6\times10^4$ cells were plated on the Lab-Tek II chamber glass cover slips (Nunc), and were grown overnight to ~80% confluence. NIH-3T3 cells were transiently transfected with 0.5 μg plasmid DNA using Lipofectamine 2000 according to the manufacturer's instructions (Invitrogen). The arylstibonic acid compound, or equal volume of 50 mM $NH_4OAc$, pH 9.0, was added 5 h after the transfection, and the cells were grown overnight.

For fluorescence imaging, transfected cells were fixed with 10% neutral buffered formalin at room temperature for 10 min. The images were captured using a Zeiss LSM 510 confocal laser scanning microscope (Carl Zeiss MicroImaging Inc).

**Cell survival assay.** K562 and CCS1 cells were seeded at $4\times10^4$ per well in RPMI media in 96-well plates. Serial dilutions of arylstibonic acid compounds in the same media were added to each well to a final 100 μl volume. Cytotoxicity was measured using the Cell Titer 96 Aqueous One Solution Cell Proliferation Assay (Promega) according to the manufacturer's protocol. Briefly, after 24–96-h of exposure, 20 μl MTS reagent was added to each well and the plates were incubated in a humidified 37 °C incubator with 5% $CO_2$ for 2–4 h until the $OD_{600}$ of untreated cells was equal to 1.0. Absorbance at 490 nM was recorded using a BioTek Power Wave XS/XS2 microplate spectrophotometer (BioTek). Data were normalized against the untreated cells to generate the dose-response curves. All experiments were performed at least three times and each sample was treated in six replicates. Statistical analysis was performed using the Student's *t*-test.

**Cell cycle analysis.** Cells were expanded in fresh media 48-h prior to the experiment, and treated for 24, 48 or 72 h with 25 μM arylstibonic acids as indicated. At the end of each time point, cells were pulsed with BrdU for 4 h, fixed and permeabilized as per manufacturer's instructions (BD Bioscience). Cells were then stained for caspase 3 using anti-active caspase 3 antibody (BD Biosciences), washed and subjected to flow cytometry using a FACS Calibur cytometer (BD Biosciences). Live-dead

Molecular Pharmacology Fast Forward. Published on July 31, 2012 as DOI: 10.1124/mol.112.080820
This article has not been copyedited and formatted. The final version may differ from this version.



discrimination was performed by staining the DNA with 7AAD, and cell aggregates were discarded from the analysis by doublet discrimination. The cell cycle analysis was performed on 50,000 cells and normalized against the untreated cells. Each arylstibonic acid compound was analyzed in biological replicates.

**Mouse xenograft of a clear cell sarcoma of soft tissue cell line.** All experiments were conducted in an Association for Assessment and Accreditation of Laboratory Animal Care accredited facility in accordance with the Public Health Service Guidelines for the Care and Use of Animals in Research. The xenograft of the CCS-1 cell line was generated by subcutaneously injecting $1\times10^6$ cells into SCID/NCr mice (BALB/c background) in a 1:1 mixture of Matrigel (BD Biosciences)/DMEM. The drug treatment began 28 days after the cell implantation, designated as time 0, when tumor mass reached between 75–150 mg. The arylstibonic acids were dissolved in DMSO, diluted in PBS and stored in aliquots at -20 °C. Treatment was performed by injecting drugs at 60 mg/kg intraperitoneally, twice a day, for four weeks. The tumor volume was determined biweekly using caliper measurements in two perpendicular dimensions (length and width). Tumor weights were calculated using the formula for a prolate ellipsoid and assuming a specific gravity of 1.0 g/cm$^3$. The experiment was terminated at day 37 when the larger tumors were determined to represent a significant burden to the mice.

## Results

### 25 Arylstibonic acids inhibit the DNA binding of B-ZIP and B-HLH-ZIP proteins.

Previously, we identified that NSC13778, an arylstibonic acid, binds to several B-ZIP proteins and inhibits their DNA binding (Rishi et al., 2010; Rishi et al., 2005). To identify additional compounds with potentially more potent properties, we screened a library of 46 arylstibonic acids obtained from the Developmental Therapeutics Program, Frederick National Laboratory for Cancer Research, for the inhibition of DNA binding of five proteins: three B-ZIPs (CREB, C/EBPα, and VBP) and two B-HLH-ZIPs (USF and Mitf) (Fig. 1). The chemical structures and DNA binding inhibition activities ($IC_{50}$) of these 46 compounds for each of the five proteins are summarized in Fig. 1 and Supplemental Table 1.

Molecular Pharmacology Fast Forward. Published on July 31, 2012 as DOI: 10.1124/mol.112.080820
This article has not been copyedited and formatted. The final version may differ from this version.



EMSA using different concentrations of compound (0.1, 0.3, 1.0, 3.0, and 10 μM) identified P6981 as the most potent arylstibonic acid in this library (Fig. 2). P6981 abolished the DNA binding of CREB and C/EBPα at 0.1 μM (Fig. 2*A*). At 1.0 μM, P6981 inhibited the DNA binding of all five proteins examined (Fig. 2*C*).

The structure-activity relationship indicates that the 12 most active compounds contain one or two carboxylic acid groups either para or meta to the stibonic acid group on the benzene ring, suggesting that the carboxylic acid group is important for inhibitory activity. Specific arylstibonic acids were found to inhibit particular B-ZIP motifs. At 0.1 μM, P6981 inhibited both CREB and C/EBPα, whereas P6982, containing two carboxylic groups para to the stibonic acid group, inhibited CREB but not C/EBPα binding to DNA (Fig. 1 and 2*A*). At 0.3 μM, P7796 was active against only CREB, P6982 was active against both CREB and VBP, and P6981 was active against all three B-ZIP proteins examined and one of the B-HLH-ZIP proteins, USF (Fig. 2*B*). At 10 μM, all 25 compounds were active against at least one of the five proteins (Fig. 2*E*). In general, the library was more active against the B-ZIPs than the B-HLH-ZIPs, and CREB|DNA complex was the easiest to be disrupted.

**P6981 inhibits CREB binding to DNA with an $IC_{50}$ ~5 nM.** To evaluate P6981 activity at the nanomolar range, EMSA were performed with P6981 against three B-ZIP proteins: CREB, C/EBPα, and C/EBPβ, a protein not included in Fig. 2 but inhibited by NSC13746 (Rishi et al., 2010). P6981 disrupted CREB at lower concentrations ($IC_{50}$ = ~5 nM) than C/EBPα ($IC_{50}$ = ~20 nM) and had little activity for C/EBPβ at 100 nM (Fig. 3, *A* and *B*; Supplemental Table 1). In contrast, NSC13746 was much more potent in the disruption of C/EBPβ|DNA complex ($IC_{50}$= ~30 nM) (Fig. 3*C*; Supplemental Table 1). The results demonstrate that arylstibonic acids have distinct inhibition specificities.

**CD spectroscopy of P6981 binding to both B-ZIP and leucine zipper domains**. Thermal denaturation curves have been extensively used to identify ligand-protein interactions (Crowther et al., 2009; Guiguemde et al., 2010; Rishi et al., 2005). Previously, we used thermal denaturations monitored by CD spectroscopy to demonstrate that NSC13778 stabilizes B-ZIP proteins (Rishi et al., 2010). The B-ZIP domain is comprised of a bipartite α-helix: the N-terminal basic region that becomes α-helical when

Molecular Pharmacology Fast Forward. Published on July 31, 2012 as DOI: 10.1124/mol.112.080820
This article has not been copyedited and formatted. The final version may differ from this version.



it interacts with DNA, and the C-terminal leucine zipper that homo- or hetero-dimerizes to form a parallel coiled coil (Krylov et al., 1998; Krylov et al., 1994; Krylov et al., 1995; Moitra et al., 1997; Moll et al., 2000; Vinson et al., 2002).

To further investigate the inhibitory mechanisms of P6981, thermal denaturations were performed using B-ZIP and leucine zipper domains (Fig. 4*A* and *B*). Increasing concentrations of P6981 were added to 2 μM VBP dimer and thermally denatured. The increasing melting temperatures of the VBP B-ZIP domain showed that P6981 increased the stability of the VBP B-ZIP domain. The leucine zipper domain is more stable than the B-ZIP domain, which indicates that the basic region destabilizes the dimer, as observed previously (Fig. 4*A* and *B*) (Moll et al., 2000). P6981 also increased the stability of VBP and CREB leucine zippers (Fig. 4*B*; Supplemental Fig. 2), suggesting that there is additional binding site(s) in the leucine zipper. P6981 did not change the thermal stability of a chimeric histone protein H2A-H2B, demonstrating that the interaction between P6981 and the B-ZIP domains is specific (Fig. 4*C*).

To evaluate possible electrostatic interactions between arylstibonic acids and B-ZIP proteins, thermal denaturation experiments using either the VBP B-ZIP or leucine zipper domain were performed at three salt concentrations (15, 150, and 2,000 mM KCl). P6981 increased the $T_m$s of the VBP B-ZIP and leucine zipper domains only at the two lower salt concentrations (Supplemental Fig. 3, right panels; Supplemental Table 2), indicating that there is an electrostatic component for the interactions between P6981 and the B-ZIP domain, as observed in the X-ray structure (see below).

**Crystal structure of NSC13778 bound to the VBP leucine zipper.** To better understand the molecular basis of the interaction between arylstibonic acids and B-ZIP proteins, we tried to crystallize both the VBP B-ZIP domain and leucine zipper bound to NSC13778, an arylstibonic acid, used because of compound availability. Crystals were only obtained with the leucine zipper. Although the two monomers of the leucine zipper dimer appear to be structurally equivalent, one NSC13778 molecule binds to only one of the two interfaces in the VBP dimer (Fig. 5). Both interfaces, with or without the arylstibonic acid, contain interhelical salt bridges between arginine and glutamic acid side-chains as previously suggested (Krylov et al., 1994). The stibonate group is coordinated between two arginine side-

Molecular Pharmacology Fast Forward. Published on July 31, 2012 as DOI: 10.1124/mol.112.080820
This article has not been copyedited and formatted. The final version may differ from this version.



chains, R20 and R27, of one peptide, which form interhelical salt bridges with glutamic acid side-chains, E15 and E22, respectively, of the other peptide of the dimer (Fig. 5, *A* and *B*). The conformational differences between the two interfaces are shown in Fig. 5*C*. The guanidinium plane of R20 is oriented for favorable interactions with both the stibonate and carboxylate groups of NSC13778. The asymmetry is generated from the "one up, one down" rotamer conformations of N16 required for their interhelical interaction, as was observed in the first coiled coil structure (O'Shea et al., 1991). The result is a polarizing effect whereby only one asparagine conformer provides the necessary side-chain network of interactions for ligand binding (N16 to E15 to R20, yellow), whereas the same set of residues on the opposing face results in an alternate network of interactions (N16 to R20 to E15, cyan), which precludes binding of the arylstibonic acid (Fig. 5*D*). The VBP|NSC13778 complex is further stabilized by simultaneous coordination of the stibonate group by both R20 and R27 (Fig. 5*A*). The guanidinium plane of R27 is also oriented for binding (Fig. 5*C*) likely by an induced fit mechanism.

The VBP leucine zipper in complex with NSC13778 crystallized in space group $P6_1$, containing one leucine zipper in the asymmetric unit. Interestingly, six leucine zippers orient head to tail in the form a hexagonal staircase structure, thereby generating the crystallographic six-fold screw axis of symmetry (Fig. 5*E*). The compound is centrally located along the long axis of the leucine zipper, and is therefore farthest away from neighboring leucine zippers in the crystal lattice. The hexagonal coils of the leucine zippers interlock to form a continuous geometric structure that, when viewed along the six-fold screw axis, depicts that of a beehive honeycomb (Fig. 5*F*).

**Inhibition of the DNA binding of nuclear extracts by arylstibonic acids.** The disruption of DNA binding of recombinant B-ZIP domains by the arylstibonic acids prompted us to assess their inhibitory activities in nuclear extracts containing native proteins. EMSAs using mouse liver nuclear extracts with the same CRE and C/EBP probes used in Fig. 2 and 25 active arylstibonic acids produced identical patterns of activity as those observed with recombinant CREB and C/EBPα B-ZIP domains (compare Fig. 2 and 6). P6981 was again identified as the most active compound. The protein|DNA complexes were disrupted with 100-fold excess of unlabeled probe, but not with 100-fold excess of DNA

Molecular Pharmacology Fast Forward. Published on July 31, 2012 as DOI: 10.1124/mol.112.080820
This article has not been copyedited and formatted. The final version may differ from this version.



containing unrelated AP1 and SP1 sequences, showing that nuclear extracts binding to the C/EBP or CRE sequences were specific (Fig. 6*B*). These results demonstrate that P6981 can inhibit biologically relevant nuclear extracts from binding to DNA containing C/EBP and CRE sequences.

**P6981 alters the subcellular localization of B-ZIP and B-HLH-ZIP proteins.** Previously, NSC13746 was shown to cause GFP-B-ZIP proteins, which reside in the nucleus under normal physiological conditions, to both move faster in the nucleus and to partially localize in the cytoplasm, demonstrating activity in cells (Heyerdahl et al., 2010). To investigate whether P6981 was also active in cells, the subcellular localization of GFP-tagged B-ZIP or B-HLH-ZIP proteins was determined by confocal microscopy. NIH-3T3 cells were transiently transfected with one of the four GFP-tagged transcription factors, including two B-ZIP proteins (C/EBPα and VBP), one B-HLH-ZIP protein (Mitf), and one hormone receptor (glucocorticoid receptor, GR) that served as a negative control. When the NIH-3T3 cells were mock-treated or treated with NSC13776, an inactive arylstibonic acid (Fig. 1), all four chimeric proteins localized to the nucleus (Fig. 7, two left panels). When the cells were incubated with 100 μM NSC13778 or P6981, cytoplasmic localization was observed for GFP-tagged C/EBPα, VBP, and Mitf (Fig. 7, two right panels), consistent with the results obtained by co-transfection of GFP-B-ZIPs and their respective dominant negative proteins that disrupt the DNA binding of specific B-ZIP proteins (Heyerdahl et al., 2010). The subcellular localization of GFP-GR was not changed, demonstrating specificity of the arylstibonic acids. Cytoplasmic localization of GFP-tagged B-ZIP proteins in the presence of P6981 and NSC13778 suggests that these compounds inhibited the DNA binding of B-ZIP proteins in cells. Neither NSC13778 nor P6981 at 100 μM altered the morphology of the transfected cells, suggesting there is no overt toxicity.

**P6981 inhibits the growth of EWS-ATF1 driven clear cell sarcoma cells.** Previously we showed that NSC13746 inhibits the growth of a cell line derived from a patient with clear cell sarcoma (CCS-1), which contains an oncogenic chimeric protein, EWS-ATF1 (Heyerdahl et al., 2010). Fusion of the B-ZIP domain of ATF1, a CREB family member (Vinson et al., 2002; Newman and Keating, 2003), with the N-terminal region of EWS leads to the constitutive binding of the chimeric protein to some CRE

Molecular Pharmacology Fast Forward. Published on July 31, 2012 as DOI: 10.1124/mol.112.080820
This article has not been copyedited and formatted. The final version may differ from this version.



sequences which drives tumorigenesis (Fujimura et al., 1996; Schaefer et al., 2004; Zucman et al., 1993). PCR analysis confirmed that the CCS-1 cells contained the in-frame fusion of EWS and ATF1 (Supplemental Fig. 4) (Panagopoulos et al., 2002). CCS-1 and the control K562 cells were incubated with increasing concentrations of three arylstibonic acids: the most active compound (P6981), a compound with moderate activity (NSC13746), and an inactive compound (NSC13776). Cell growth was measured after four days (Fig. 8). P6981 was more effective than NSC13746 in suppressing CCS-1 growth (Fig. 8*A* and *B*), consistent with the EMSA results (Fig. 3). A ~50% decrease in the proliferation of CCS-1 by P6981 was observed at 25–100 μM, whereas NSC13746 decreased the proliferation of CCS-1 only by ~25% at 100 μM. NCS13776 was inactive at all tested concentrations, suggesting that inhibition of the B-ZIP domain of the EWS-ATF1 chimera drives the observed growth inhibition effect and that it is not a non-specific effect of the arylstibonic acids (Fig. 2 and 8). The arylstibonic acids did not decreased the growth of K562 leukemia cells, which bears the Bcr-Abl fusion protein, a constitutively active tyrosine kinase unrelated to B-ZIP transcription factors (Sawyers, 1999), arguing for the specificity of function.

**Cell cycle arrest of CCS-1 by P6981.** We next examined the cell cycle profile of CCS-1 cells at 24, 48, and 72 h following a single dose of 25 μM P6981, NSC13778, or NSC13776 (Fig. 9*A* and *B*). We used the bromodeoxyuridine (BrdU) pulse exposure to identify cells in S phase and used 7-aminoactinomycin D (7AAD) to label the total DNA. Cell cycle analysis showed that P6981 produced a 50% reduction in S phase at 24 h of treatment that persisted until 48 h with a concomitant increase in $G_1/G_0$ phase (Fig. 9*A* and *B*). In contrast, NSC13778 produced a more modest and transient S phase suppression that lasted for only 24 h without the $G_1/G_0$ arrest. The inactive NSC13776 did not cause any changes in cell cycle. To study the effect of the arylstibonic acid compounds on apoptosis, the active caspase 3 was quantified (Supplemental Fig. 5). There were no detectable changes in the active caspase staining, in agreement with a cytostatic mode of action for these compounds. However, caspase 3 deficiency in CCS-1 cannot be ruled out, as is well-documented for other human cancer cell lines, such as

Molecular Pharmacology Fast Forward. Published on July 31, 2012 as DOI: 10.1124/mol.112.080820
This article has not been copyedited and formatted. The final version may differ from this version.



MCF-7 breast carcinoma cells (Janicke et al., 1998). In conclusion, P6981 has a cytostatic effect on cell cycle progression.

**Growth inhibition of xenografted CCS-1 by NSC13778.** To evaluate whether the arylstibonic acids can decrease the growth of EWS-ATF1 containing CCS-1 cells *in vivo*, $1\times10^6$ cells were injected subcutaneously into immunocompromised SCID/NCr mice to generate a xenograft model. Due to availability, NSC13778 was administered intraperitoneally twice a day at 60 mg/kg to randomly selected mice, and the control group was treated with vehicle buffer. Tumor volumes were measured on day 37 after the beginning of the treatment, and control and treated groups were compared (Fig. 9*C*). NSC13778 treatment did not result in loss of body weight (Supplemental Table 4), and no signs of toxicity were apparent. The tumor growth was inhibited in four of the five mice treated with NSC13778, and the average tumor volume of the control group was 80% higher than that of the treatment group. Only one of five tumors in the NSC13778-treated group grew larger, and that tumor was already the largest (~150 mg) at the beginning of the therapy. These results suggest that the arylstibonic acid NSC13778 decreased the growth of CCS-1 derived xenograft tumors, consistent with what was observed in both cell survival and cell cycle experiments (Fig. 8 and 9).

## Discussion

Using EMSA to measure inhibition of the DNA binding to three B-ZIP (CREB, C/EBPα, and VBP) and two B-HLH-ZIP (USF and Mitf) proteins, we report that 25 of the 46 arylstibonic acids screened were active at a concentration of 10 μM. P6981, the most potent compound in this arylstibonic acid library, inhibited DNA binding of CREB and C/EBPα with $IC_{50}$ values of ~5 and 20 nM, respectively. P6981 bound to both the B-ZIP and the leucine zipper domains. P6981 does not inhibit the growth of K562 cells but does inhibit the growth of a patient derived clear cell sarcoma cell line driven by a chimeric protein containing the B-ZIP domain of ATF1. Presently, there are no compounds in clinical use that inhibit the DNA binding of B-ZIP proteins. The data presented here suggest that arylstibonic acids could potentially address this therapeutic void.

Molecular Pharmacology Fast Forward. Published on July 31, 2012 as DOI: 10.1124/mol.112.080820
This article has not been copyedited and formatted. The final version may differ from this version.



To gain insight into the inhibitory effects of arylstibonic acids on DNA binding, we analyzed the structure-activity relationship (SAR). Two carboxylic acid groups attached to the phenyl ring via an ethyl group yields the most active arylstibonic acids, P6981 and P6982. The ethyl linkage appears to be important for their inhibitory activities, since P6954 and P6966, which have two carboxylic acid groups directly attached to the phenyl ring, are much less active. Similar effects were observed by the Stivers group when arylstibonic acids were screened for Ape1 inhibitors (Seiple et al., 2008), although a different set of compounds were found to be active (see below). In addition, the compounds with carboxylic acid groups on the phenyl ring meta to the stibonic acid group are more active than those with carboxylic acid groups at the para positions (compare NSC13778, NSC732942 vs. NSC732943; P6981 vs. P6982; NSC13759 vs. NSC13760).

Arylstibonic acids have been recently identified in several small-molecule screens. NSC13778 was reported to have anti-HIV activity, mediated by binding to CD4 on cell surfaces and thus interfering with viral gp120 binding and virus entry (Yang et al., 2005). Stivers and colleagues recently showed that arylstibonic acids inhibit type I DNA topoisomerases (human and poxvirus Topo) and apurinic/apyrimidinic endonuclease (Ape1) (Kim et al., 2008; Seiple et al., 2008). Different arylstibonic acids showed different activities in these screens. In the screens for Topo inhibitors, P6981 was one of the least active arylstibonic acids to inhibit poxvirus Topo in a supercoil relaxation assay. P6981 even showed a slightly stimulatory effect on human Topo (Kim et al., 2008). In a molecular beacon high-throughput assay where the abasic DNA cleavage activity of Ape1 was assessed, P6981 also failed to inhibit Ape1 activity by $\geq$50% at a concentration as high as 10 $\mu$M (Seiple et al., 2008). In contrast, P6954, P6970, NSC13755, and NSC13759, the most potent inhibitors of Topo or Ape1, are relatively weak inhibitors of the B-ZIP and B-HLH-ZIP proteins examined in our study (Fig. 1 and 2). These data suggest that arylstibonic acids have specific activities for distinct molecular targets.

CD thermal denaturations suggest that P6981 may have binding sites on both the basic region and leucine zipper of the VBP B-ZIP domain (Fig. 4). Moreover, Kim *et al.* proposed that the structural similarity between arylstibonic acid and phosphate of B-DNA could explain the multiple binding sites of

Molecular Pharmacology Fast Forward. Published on July 31, 2012 as DOI: 10.1124/mol.112.080820
This article has not been copyedited and formatted. The final version may differ from this version.



an arylstibonic acid on a DNA binding protein (Kim et al., 2008). This is further supported in the VBP39-NSC13778 crystal structure showing the stibonate group of NSC13778 is bound between two arginines in a phosphate-like coordination. Previous work has mapped the binding of NSC13778 to the region between the basic region and the leucine zipper (Rishi et al., 2005). A structure of the B-ZIP domain bound to NSC13778 is being pursued.

Both USF and CREB activate the *Helicobacter pylori*-induced COX-2 gene expression, contributing to ulcers and gastric cancers (Juttner et al., 2003). Furthermore, in the clear cell sarcoma cells, the constitutively active EWS-ATF1 chimera induces Mitf expression via the B-ZIP domain of ATF1, and Mitf in turn maintains proliferation of the tumor cells (Davis et al., 2006). The pleiotropic effect, or polypharmacology (Dar et al., 2012; Knight et al., 2010), of P6981 on B-ZIPs and B-HLH-ZIPs may be desirable for therapeutic intervention of cancer, since two or more of these transcription factors often regulate the same gene expression pathways implicated in pathogenic conditions.

It is worth noting that P6981 was less potent in cells than *in vitro*, which could result from its possible low stability in cells, and/or off-target effects that could counteract its B-ZIP inhibition activity. Nonetheless, the xenograft mouse data suggest that NSC13778, a P6981 analog, was able to decrease the growth of clear cell sarcoma *in vivo* without toxicity.

In summary, we have characterized the inhibitory effects of 46 arylstibonic acids, and identified P6981 as a potent inhibitor that disrupted CREB and C/EBPα|DNA complexes at nanomolar concentrations. This compound also inhibited VBP, USF and Mitf binding to their target DNA sequences. To our knowledge, this is the first report that identifies a small-molecule inhibitor of USF and Mitf, the B-HLH-ZIP proteins. More importantly, P6981 demonstrated substantially improved efficacy in suppressing the growth of a clear cell sarcoma cell line, as compared to the previously reported NSC13746 compound. Although still rare, a diverse group of neoplasms containing EWS-ATF1 or EWS-CREB is being detected at an increasing frequency, and therefore requires attention to development of molecularly targeted therapies (Thway and Fisher, 2012). The combination of P6981 that inhibits the

Molecular Pharmacology Fast Forward. Published on July 31, 2012 as DOI: 10.1124/mol.112.080820
This article has not been copyedited and formatted. The final version may differ from this version.



DNA binding of B-ZIP transcription factors, including CREB and ATF1, with other anticancer compounds may be a promising approach to increasing treatment efficacy.

Molecular Pharmacology Fast Forward. Published on July 31, 2012 as DOI: 10.1124/mol.112.080820
This article has not been copyedited and formatted. The final version may differ from this version.



**Authorship Contributions**

Participated in research design: Zhao, Stagno, Rishi, Shoemaker, Ji, and Vinson.

Conducted experiments: Zhao, Stagno, Nimako, Varticovski, McKinnon, and Akee.

Performed data analysis: Zhao, Stagno, Varticovski, McKinnon, and Akee.

Wrote or contributed to the writing of the manuscript: Zhao, Stagno, Akee, Varticovski, McKinnon, Shoemaker, Ji, and Vinson.

Molecular Pharmacology Fast Forward. Published on July 31, 2012 as DOI: 10.1124/mol.112.080820
This article has not been copyedited and formatted. The final version may differ from this version.



**References**

Adams PD, Grosse-Kunstleve RW, Hung LW, Ioerger TR, McCoy AJ, Moriarty NW, Read RJ, Sacchettini JC, Sauter NK and Terwilliger TC (2002) PHENIX: building new software for automated crystallographic structure determination. *Acta Crystallogr D Biol Crystallogr* **58**(Pt 11):1948-1954.

Ahn S, Olive M, Aggarwal S, Krylov D, Ginty DD and Vinson C (1998) A dominant-negative inhibitor of CREB reveals that it is a general mediator of stimulus-dependent transcription of c-fos. *Mol Cell Biol* **18**(2):967-977.

Bonci A and Carlezon WA, Jr. (2005) Ion channels and intracellular signaling proteins as potential targets for novel therapeutics for addictive and depressive disorders. *Pharmacol Ther* **108**(1):65-75.

Chen VB, Arendall WB, 3rd, Headd JJ, Keedy DA, Immormino RM, Kapral GJ, Murray LW, Richardson JS and Richardson DC (2010) MolProbity: all-atom structure validation for macromolecular crystallography. *Acta Crystallogr D Biol Crystallogr* **66**(Pt 1):12-21.

Corre S and Galibert MD (2005) Upstream stimulating factors: highly versatile stress-responsive transcription factors. *Pigment Cell Res* **18**(5):337-348.

Crowther GJ, Napuli AJ, Thomas AP, Chung DJ, Kovzun KV, Leibly DJ, Castaneda LJ, Bhandari J, Damman CJ, Hui R, Hol WG, Buckner FS, Verlinde CL, Zhang Z, Fan E and van Voorhis WC (2009) Buffer optimization of thermal melt assays of Plasmodium proteins for detection of small-molecule ligands. *J Biomol Screen* **14**(6):700-707.

Dar AC, Das TK, Shokat KM and Cagan RL Chemical genetic discovery of targets and anti-targets for cancer polypharmacology (2012). *Nature* **486**(7401):80-84.

Davis IJ, Kim JJ, Ozsolak F, Widlund HR, Rozenblatt-Rosen O, Granter SR, Du J, Fletcher JA, Denny CT, Lessnick SL, Linehan WM, Kung AL and Fisher DE (2006) Oncogenic MITF dysregulation in clear cell sarcoma: defining the MiT family of human cancers. *Cancer Cell* **9**(6):473-484.

Fujimura Y, Ohno T, Siddique H, Lee L, Rao VN and Reddy ES (1996) The EWS-ATF-1 gene involved in malignant melanoma of soft parts with t(12;22) chromosome translocation, encodes a constitutive transcriptional activator. *Oncogene* **12**(1):159-167.

Gerdes MJ, Myakishev M, Frost NA, Rishi V, Moitra J, Acharya A, Levy MR, Park SW, Glick A, Yuspa SH and Vinson C (2006) Activator protein-1 activity regulates epithelial tumor cell identity. *Cancer Res* **66**(15):7578-7588.

Giuliano S, Cheli Y, Ohanna M, Bonet C, Beuret L, Bille K, Loubat A, Hofman V, Hofman P, Ponzio G, Bahadoran P, Ballotti R and Bertolotto C (2010) Microphthalmia-associated transcription factor controls the DNA damage response and a lineage-specific senescence program in melanomas. *Cancer Res* **70**(9):3813-3822.

Guiguemde WA, Shelat AA, Bouck D, Duffy S, Crowther GJ, Davis PH, Smithson DC, Connelly M, Clark J, Zhu F, Jimenez-Diaz MB, Martinez MS, Wilson EB, Tripathi AK, Gut J, Sharlow ER, Bathurst I, El Mazouni F, Fowble JW, Forquer I, McGinley PL, Castro S, Angulo-Barturen I, Ferrer S, Rosenthal PJ, Derisi JL, Sullivan DJ, Lazo JS, Roos DS, Riscoe MK, Phillips MA, Rathod PK, Van Voorhis WC, Avery VM and Guy RK (2010) Chemical genetics of Plasmodium falciparum. *Nature* **465**(7296):311-315.

Heyerdahl SL, Rozenberg J, Jamtgaard L, Rishi V, Varticovski L, Akah K, Scudiero D, Shoemaker RH, Karpova TS, Day RN, McNally JG and Vinson C (2010) The arylstibonic acid compound NSC13746 disrupts B-ZIP binding to DNA in living cells. *Eur J Cell Biol* **89**(7):564-573.

Janicke RU, Sprengart ML, Wati MR and Porter AG (1998) Caspase-3 is required for DNA fragmentation and morphological changes associated with apoptosis. *J Biol Chem* **273**(16):9357-9360.

Juttner S, Cramer T, Wessler S, Walduck A, Gao F, Schmitz F, Wunder C, Weber M, Fischer SM, Schmidt WE, Wiedenmann B, Meyer TF, Naumann M and Hocker M (2003) Helicobacter pylori stimulates host cyclooxygenase-2 gene transcription: critical importance of MEK/ERK-dependent activation of USF1/-2 and CREB transcription factors. *Cell Microbiol* **5**(11):821-834.

Kabsch W (2010) Xds. *Acta Crystallogr D Biol Crystallogr* **66**(Pt 2):125-132.

Kim H, Cardellina JH, 2nd, Akee R, Champoux JJ and Stivers JT (2008) Arylstibonic acids: novel inhibitors and activators of human topoisomerase IB. *Bioorg Chem* **36**(4):190-197.

Knight ZA, Lin H and Shokat KM (2010) Targeting the cancer kinome through polypharmacology. *Nat Rev Cancer* **10**(2):130-137.

Krylov D, Barchi J and Vinson C (1998) Inter-helical interactions in the leucine zipper coiled coil dimer: pH and salt dependence of coupling energy between charged amino acids. *J Mol Biol* **279**(4):959-972.

Krylov D, Mikhailenko I and Vinson C (1994) A thermodynamic scale for leucine zipper stability and dimerization specificity: e and g interhelical interactions. *EMBO J* **13**(12):2849-2861.

Krylov D, Olive M and Vinson C (1995) Extending dimerization interfaces: the bZIP basic region can form a coiled coil. *EMBO J* **14**(21):5329-5337.

Lu M, Shu W, Ji H, Spek E, Wang L and Kallenbach NR (1999) Helix capping in the GCN4 leucine zipper. *J Mol Biol* **288**(4):743-752.

Massari ME and Murre C (2000) Helix-loop-helix proteins: regulators of transcription in eucaryotic organisms. *Mol Cell Biol* **20**(2):429-440.

Mayr B and Montminy M (2001) Transcriptional regulation by the phosphorylation-dependent factor CREB. *Nat Rev Mol Cell Biol* **2**(8):599-609.

Moitra J, Szilak L, Krylov D and Vinson C (1997) Leucine is the most stabilizing aliphatic amino acid in the d position of a dimeric leucine zipper coiled coil. *Biochemistry* **36**(41):12567-12573.

Moll JR, Olive M and Vinson C (2000) Attractive interhelical electrostatic interactions in the proline- and acidic-rich region (PAR) leucine zipper subfamily preclude heterodimerization with other basic leucine zipper subfamilies. *J Biol Chem* **275**(44):34826-34832.

Nerlov C (2008) C/EBPs: recipients of extracellular signals through proteome modulation. *Curr Opin Cell Biol* **20**(2):180-185.

Newman JR and Keating AE (2003) Comprehensive identification of human bZIP interactions with coiled-coil arrays. *Science* **300**(5628):2097-2101.

O'Shea EK, Klemm JD, Kim PS and Alber T (1991) X-ray structure of the GCN4 leucine zipper, a two-stranded, parallel coiled coil. *Science* **254**(5031):539-544.

Oh WJ, Rishi V, Orosz A, Gerdes MJ and Vinson C (2007) Inhibition of CCAAT/enhancer binding protein family DNA binding in mouse epidermis prevents and regresses papillomas. *Cancer Res* **67**(4):1867-1876.

Olive M, Krylov D, Echlin DR, Gardner K, Taparowsky E and Vinson C (1997) A dominant negative to activation protein-1 (AP1) that abolishes DNA binding and inhibits oncogenesis. *J Biol Chem* **272**(30):18586-18594.

Panagopoulos I, Mertens F, Debiec-Rychter M, Isaksson M, Limon J, Kardas I, Domanski HA, Sciot R, Perek D, Crnalic S, Larsson O and Mandahl N (2002) Molecular genetic characterization of the EWS/ATF1 fusion gene in clear cell sarcoma of tendons and aponeuroses. *Int J Cancer* **99**(4):560-567.

Rishi V, Gal J, Krylov D, Fridriksson J, Boysen MS, Mandrup S and Vinson C (2004) SREBP-1 dimerization specificity maps to both the helix-loop-helix and leucine zipper domains: use of a dominant negative. *J Biol Chem* **279**(12):11863-11874.

Rishi V, Oh WJ, Heyerdahl SL, Zhao J, Scudiero D, Shoemaker RH and Vinson C (2010) 12 Arylstibonic acids that inhibit the DNA binding of five B-ZIP dimers. *J Struct Biol* **170**(2):216-225.

Rishi V, Potter T, Laudeman J, Reinhart R, Silvers T, Selby M, Stevenson T, Krosky P, Stephen AG, Acharya A, Moll J, Oh WJ, Scudiero D, Shoemaker RH and Vinson C (2005) A high-throughput fluorescence-anisotropy screen that identifies small molecule inhibitors of the DNA binding of B-ZIP transcription factors. *Anal Biochem* **340**(2):259-271.

Rozenberg J, Rishi V, Orosz A, Moitra J, Glick A and Vinson C (2009) Inhibition of CREB function in mouse epidermis reduces papilloma formation. *Mol Cancer Res* **7**(5):654-664.

Sawyers CL (1999) Chronic myeloid leukemia. *N Engl J Med* **340**(17):1330-1340.

Schaefer KL, Brachwitz K, Wai DH, Braun Y, Diallo R, Korsching E, Eisenacher M, Voss R, Van Valen F, Baer C, Selle B, Spahn L, Liao SK, Lee KA, Hogendoorn PC, Reifenberger G, Gabbert HE and Poremba C (2004) Expression profiling of t(12;22) positive clear cell sarcoma of soft tissue cell lines reveals characteristic up-regulation of potential new marker genes including ERBB3. *Cancer Res* **64**(10):3395-3405.

Seiple LA, Cardellina JH, 2nd, Akee R and Stivers JT (2008) Potent inhibition of human apurinic/apyrimidinic endonuclease 1 by arylstibonic acids. *Mol Pharmacol* **73**(3):669-677.

Shankar DB, Cheng JC, Kinjo K, Federman N, Moore TB, Gill A, Rao NP, Landaw EM and Sakamoto KM (2005) The role of CREB as a proto-oncogene in hematopoiesis and in acute myeloid leukemia. *Cancer Cell* **7**(4):351-362.

Shukla A, Bosenberg MW, MacPherson MB, Butnor KJ, Heintz NH, Pass HI, Carbone M, Testa JR and Mossman BT (2009) Activated cAMP response element binding protein is overexpressed in human mesotheliomas and inhibits apoptosis. *Am J Pathol* **175**(5):2197-2206.

Thway K and Fisher C (2012) Tumors With EWSR1-CREB1 and EWSR1-ATF1 Fusions: The Current Status. *Am J Surg Pathol*. **36**(7):e1-e11.

Vinson C, Myakishev M, Acharya A, Mir AA, Moll JR and Bonovich M (2002) Classification of human B-ZIP proteins based on dimerization properties. *Mol Cell Biol* **22**(18):6321-6335.

Vinson CR and Garcia KC (1992) Molecular model for DNA recognition by the family of basic-helix-loop-helix-zipper proteins. *New Biol* **4**(4):396-403.

Vinson CR, Sigler PB and McKnight SL (1989) Scissors-grip model for DNA recognition by a family of leucine zipper proteins. *Science* **246**(4932):911-916.

Walton KM, Rehfuss RP, Chrivia JC, Lochner JE and Goodman RH (1992) A dominant repressor of cyclic adenosine 3',5'-monophosphate (cAMP)-regulated enhancer-binding protein activity inhibits the cAMP-mediated induction of the somatostatin promoter in vivo. *Mol Endocrinol* **6**(4):647-655.

Widlund HR and Fisher DE (2003) Microphthalamia-associated transcription factor: a critical regulator of pigment cell development and survival. *Oncogene* **22**(20):3035-3041.

Xiao X, Li BX, Mitton B, Ikeda A and Sakamoto KM (2010) Targeting CREB for cancer therapy: friend or foe. *Curr Cancer Drug Targets* **10**(4):384-391.

Xie S, Price JE, Luca M, Jean D, Ronai Z and Bar-Eli M (1997) Dominant-negative CREB inhibits tumor growth and metastasis of human melanoma cells. *Oncogene* **15**(17):2069-2075.

Yang QE, Stephen AG, Adelsberger JW, Roberts PE, Zhu WM, Currens MJ, Feng YX, Crise BJ, Gorelick RJ, Rein AR, Fisher RJ, Shoemaker RH and Sei S (2005) Discovery of small-molecule human immunodeficiency virus type 1 entry inhibitors that target the gp120-binding domain of CD4. *J Virol* **79**(10):6122-6133.

Zucman J, Delattre O, Desmaze C, Epstein AL, Stenman G, Speleman F, Fletchers CD, Aurias A and Thomas G (1993) EWS and ATF-1 gene fusion induced by t(12;22) translocation in malignant melanoma of soft parts. *Nat Genet* **4**(4):341-345.

Molecular Pharmacology Fast Forward. Published on July 31, 2012 as DOI: 10.1124/mol.112.080820
This article has not been copyedited and formatted. The final version may differ from this version.



**Footnotes**

This research was supported by the Intramural Research Program of the Center for Cancer Research, National Cancer Institute, National Institutes of Health.

Molecular Pharmacology Fast Forward. Published on July 31, 2012 as DOI: 10.1124/mol.112.080820
This article has not been copyedited and formatted. The final version may differ from this version.



**Figure Legends**

**Fig. 1.** Chemical structures of 46 arylstibonic acids. A summary of inhibitory activities of arylstibonic acids determined by EMSA. The 34 new compounds that were not present in our previous study (Rishi et al., 2010) are labeled in boldface. The 21 arylstibonic acids listed in the lower section were not soluble in the experimental conditions (italics), or did not inhibit the DNA binding of B-ZIP and B-HLH-ZIP proteins.

**Fig. 2.** Inhibitory effects of the 25 most active arylstibonic acids on DNA binding of three B-ZIP (CREB, C/EBPα and VBP) and two B-HLH-ZIP (Mitf and USF) proteins. EMSA showing the protein|DNA bands at five arylstibonic-acid concentrations: 0.1, 0.3, 1, 3, and 10 μM. Each sample included 10 nM protein dimer and 7 pM $^{32}$P-labeled 28-bp DNA probe containing the consensus binding site of each protein, except for the "DNA only" lane. The protein|DNA complexes were resolved on 7.5% native gels.

**Fig. 3.** Specificity of NSC13746 and P6981 in the inhibition of the DNA binding of unique B-ZIP domains. 15 nM dimer of C/EBPβ (*A*), C/EBPα (*B*), or CREB (*C*) B-ZIP protein was incubated with increasing concentrations of P6981 or NSC13746 (18, 32, 56, 100 nM for C/EBPβ; 5.6, 10, 18, 32, 56, 100 nM for CREB and C/EBPα) and assayed by EMSA. $IC_{50}$ values were estimated and shown in Supplemental Table 1.

**Fig. 4.** Circular dichroism at 222 nm of the thermal stabilization of the VBP B-ZIP domain dimer by P6981. *A-B*, upper panels, Thermal denaturations of 2 μM VBP B-ZIP domain dimer or leucine zipper-only dimer either alone (○); or with 10 μM (●), 25 μM (□), 50 μM (+), or 100 μM (Δ) P6981. Lower panels, $T_m$ derived from the thermal denaturations was plotted against the P6981 concentrations. *C*, Thermal denaturations of 1 μM chimeric histone protein H2A-H2B either alone ○, or with 25 μM P6981, ●.

Molecular Pharmacology Fast Forward. Published on July 31, 2012 as DOI: 10.1124/mol.112.080820
This article has not been copyedited and formatted. The final version may differ from this version.



**Fig. 5.** Crystal structure of the VBP leucine zipper (VBP39) in complex with NSC13778, color-coded by chain (chain A, magenta; chain B, green). *A*, The overall structure showing six salt bridges (three per peptide) R8/E13, E15/R20, E22/R27, asparagine bridge (N16), disulfide bridge (C33), and NSC13778 bound to one face of the coiled coil. *B*, Same as *A* but rotated 180° about the horizontal axis. The asparagine-asparagine interaction is asymmetric. *C*, Superposition of bound (yellow) and unbound (cyan) interfaces, showing the differences in side-chain conformations. *D*, Interhelical N16 interaction creates a polarizing effect whereby only one conformer provides the necessary side-chain network of interactions for ligand binding (N16 to E15 to R20, yellow). The same set of residues on the opposing face results in an alternate network of interactions (N16 to R20 to E15, cyan), which precludes binding of the compound. *E*, The VBP leucine zippers arrange head to tail to form a hexagonal staircase, which defines the crystallographic six-fold screw axis of symmetry. The bound molecules of NSC13778 are shown in blue. *F*, The crystal lattice. The hexagonal coils of the leucine zippers interlock to form a continuous geometric structure that resembles a beehive honeycomb when viewed along the six-fold screw axis of symmetry. Each vertex is the interlocking interface of three adjacent hexagonal coils.

**Fig. 6.** EMSAs using mouse liver nuclear extracts show that specific arylstibonic acids inhibit the binding of C/EBP or CRE-containing DNA. *A*, The $^{32}$P-labeled C/EBP (upper panel) or CRE (lower panel) DNA probe (lane 1) was incubated with mouse liver nuclear extracts in the absence (lane 2) or presence (lanes 3-27) of 100 μM arylstibonic acids. *B*, Competition assay using nuclear extracts and three unlabeled DNA probes at 100-fold molar excess.

**Fig. 7.** P6981 causes cytoplasmic localization of C/EBPα, VBP and Mitf, but not GR. NIH-3T3 cells were transfected with GFP-tagged C/EBPα (*A*), VBP (*B*), Mitf (*C*), or GR (*D*), and were mock treated (50 mM $NH_4OAc$, pH 9.0) or treated with 100 μM NSC13776, NSC13778, or P6981. GR served as a negative control. The confocal images are representative of three independent experiments.

Molecular Pharmacology Fast Forward. Published on July 31, 2012 as DOI: 10.1124/mol.112.080820
This article has not been copyedited and formatted. The final version may differ from this version.



**Fig. 8.** P6981 inhibits the growth of CCS-1, a clear cell sarcoma cell line containing the EWS-ATF1 chimera. CCS-1 and the control K562 cells were incubated with P6981 (*A*), NSC13746 (*B*), or NSC13776 (*C*) at 1:2 serially diluted concentrations up to 100 μM. The cell growth was monitored by MTS assay at the end of 96 h. Data shown are the average of triplicates. Error bars indicate S.D.

**Fig. 9.** P6981 induced CCS-1 growth arrest and inhibited xenografted tumor growth *in vivo*. *A*, Changes in S phase when CCS-1 cells were untreated (♦) or treated with three compounds at 25 μM for 24, 48, and 72 h: P6981 (▲), NSC13778 (■) or NSC13776 (●). Each sample was analyzed in biological replicates. *B*, Changes in $G_1/G_0$ phase after treatment described in *A*. *C*, CCS-1 cells were implanted subcutaneously into immunocompromised SCID/NCr mice, and the tumor sizes of NSC13778 (●) and vehicle control (♦) treated mice were measured on day 37 post treatment. The bars indicate the average tumor volume.

Molecular Pharmacology Fast Forward. Published on July 31, 2012 as DOI: 10.1124/mol.112.080820
This article has not been copyedited and formatted. The final version may differ from this version.

# Fig. 1

## Active at 0.1 μM

**NSC732942**

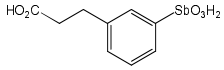

**P6970**

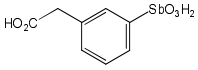

**P6971**

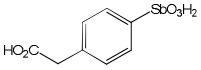

**P6981**

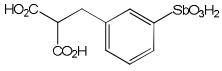

**P6982**

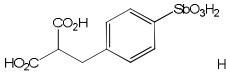

**P6987**

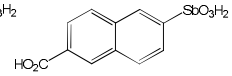

**P7794**

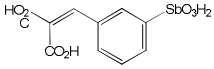

**P7795**

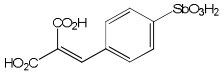

**P7796**

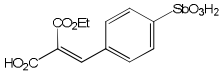

NSC13755

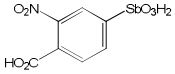

NSC13759

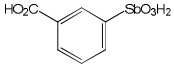

NSC13778

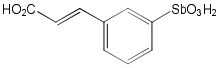

## Active at between 0.3 and 10 μM

**NSC13771**

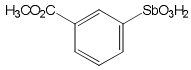

**NSC15578**

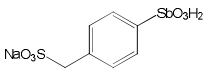

**NSC732943**

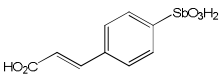

**P6953**

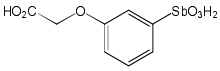

**P6954**

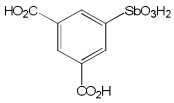

**P6964**

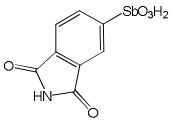

**P6966**

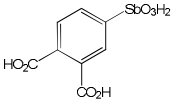

**P6968**

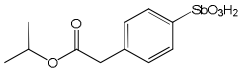

NSC13746

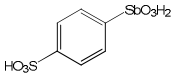

NSC13760

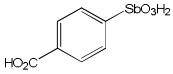

NSC13765

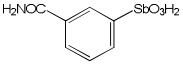

NSC13782

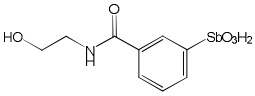

NSC13793

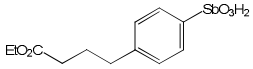

## Inactive at 10 μM

***NSC13730***

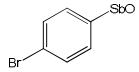

***NSC13731***

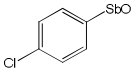

***NSC13741***

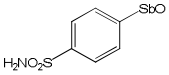

**NSC13744**

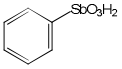

**NSC13745**

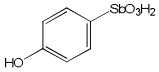

***NSC13749***

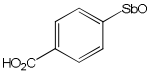

**NSC13758**

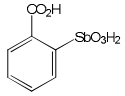

***NSC15408***

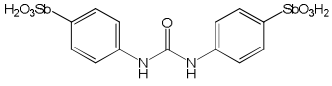

***NSC15591***

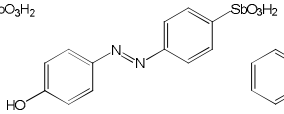

***NSC15596***

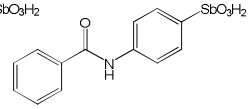

***NSC115831***

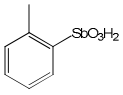

***P6952***

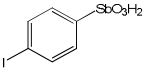

**P6965**

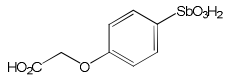

***P6967***

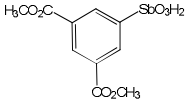

***P6972***

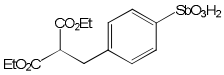

***P6983***



**4452-34-2**



*NSC13740*



*NSC13743*



NSC13776



NSC13794

Molecular Pharmacology Fast Forward. Published on July 31, 2012 as DOI: 10.1124/mol.112.080820
This article has not been copyedited and formatted. The final version may differ from this version.

Fig. 2

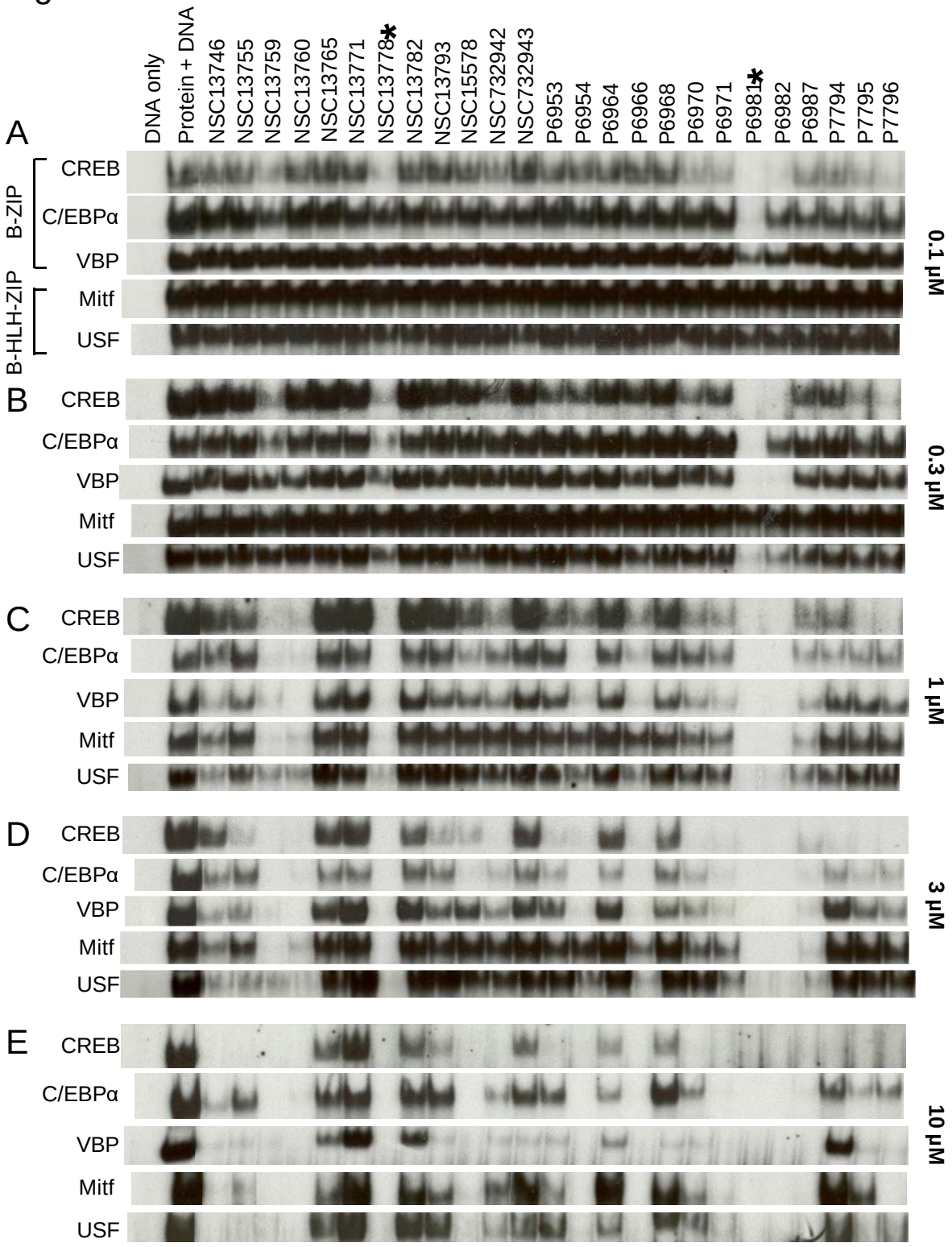

Molecular Pharmacology Fast Forward. Published on July 31, 2012 as DOI: 10.1124/mol.112.080820
This article has not been copyedited and formatted. The final version may differ from this version.

Fig. 3

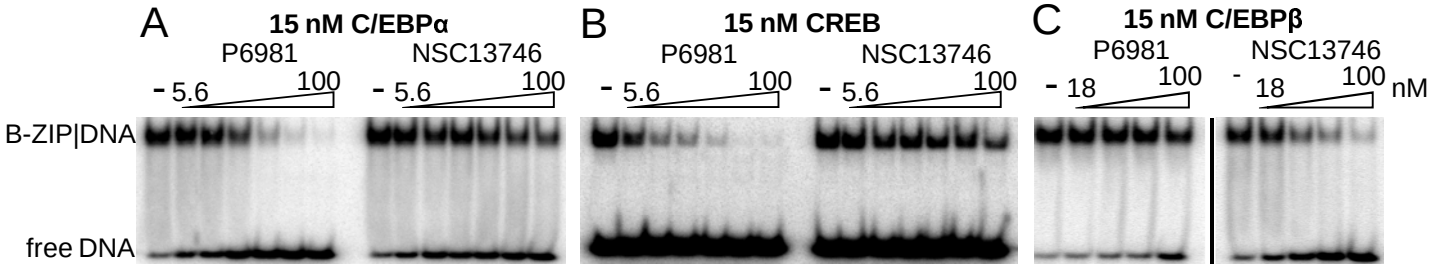

Molecular Pharmacology Fast Forward. Published on July 31, 2012 as DOI: 10.1124/mol.112.080820
This article has not been copyedited and formatted. The final version may differ from this version.

Fig. 4

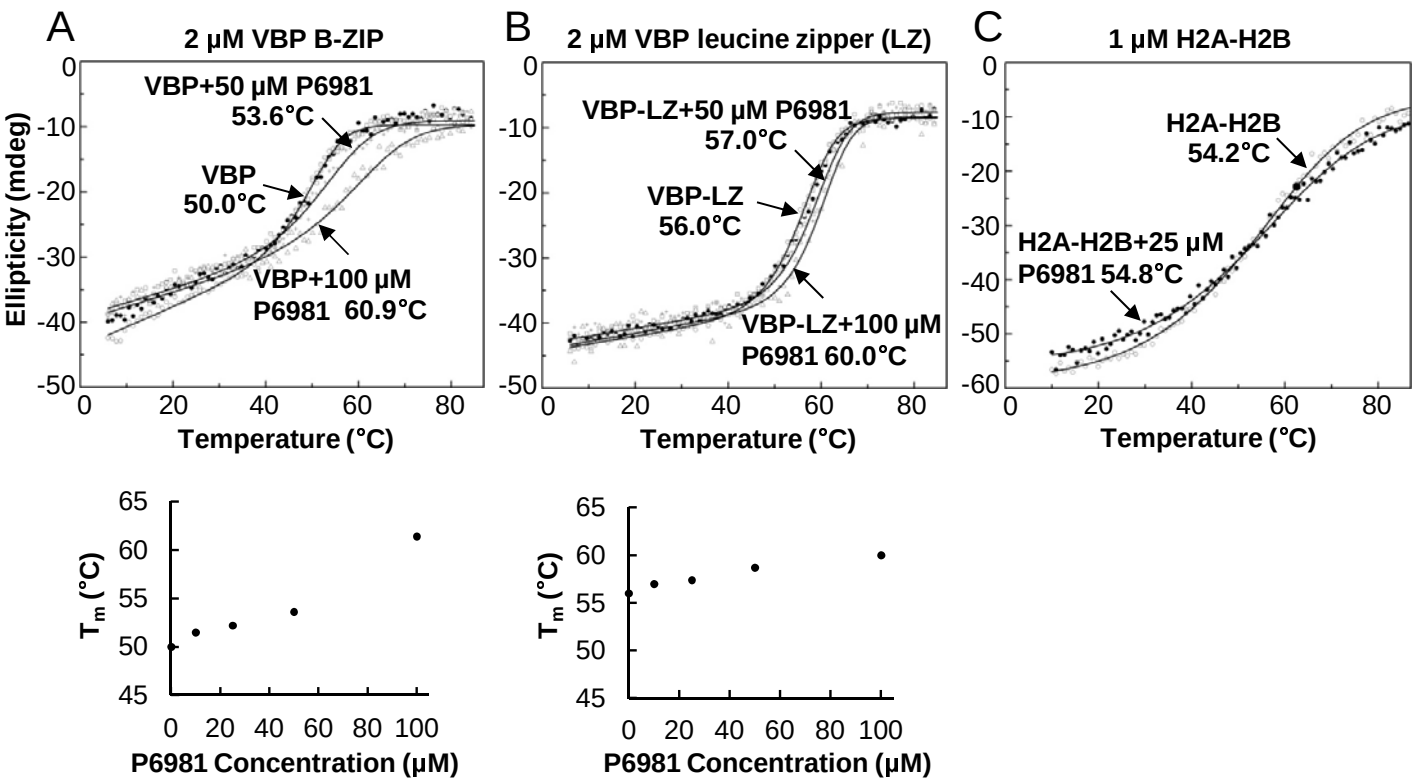

Molecular Pharmacology Fast Forward. Published on July 31, 2012 as DOI: 10.1124/mol.112.080820
This article has not been copyedited and formatted. The final version may differ from this version.

Fig. 5

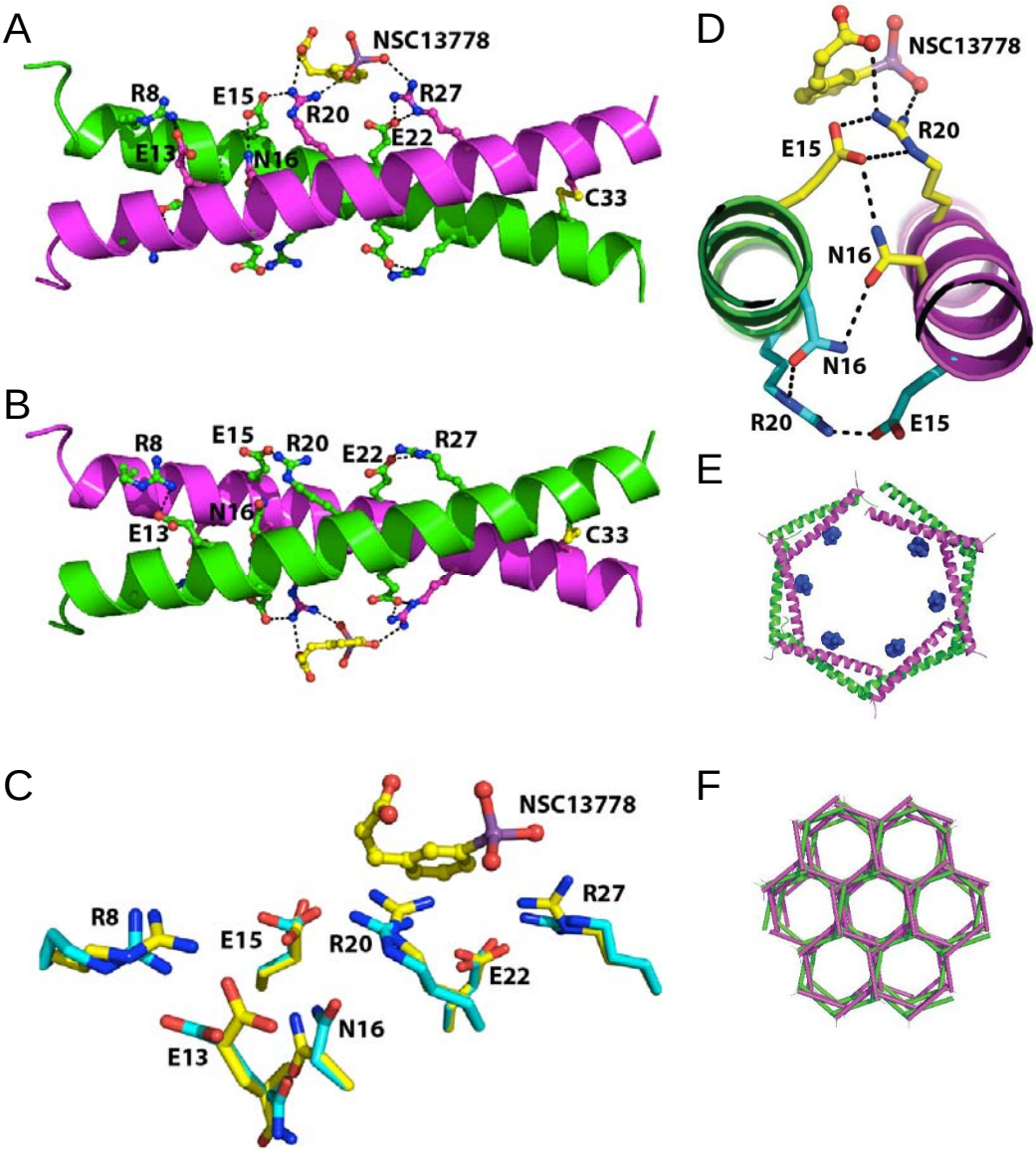

Molecular Pharmacology Fast Forward. Published on July 31, 2012 as DOI: 10.1124/mol.112.080820
This article has not been copyedited and formatted. The final version may differ from this version.

Fig. 6

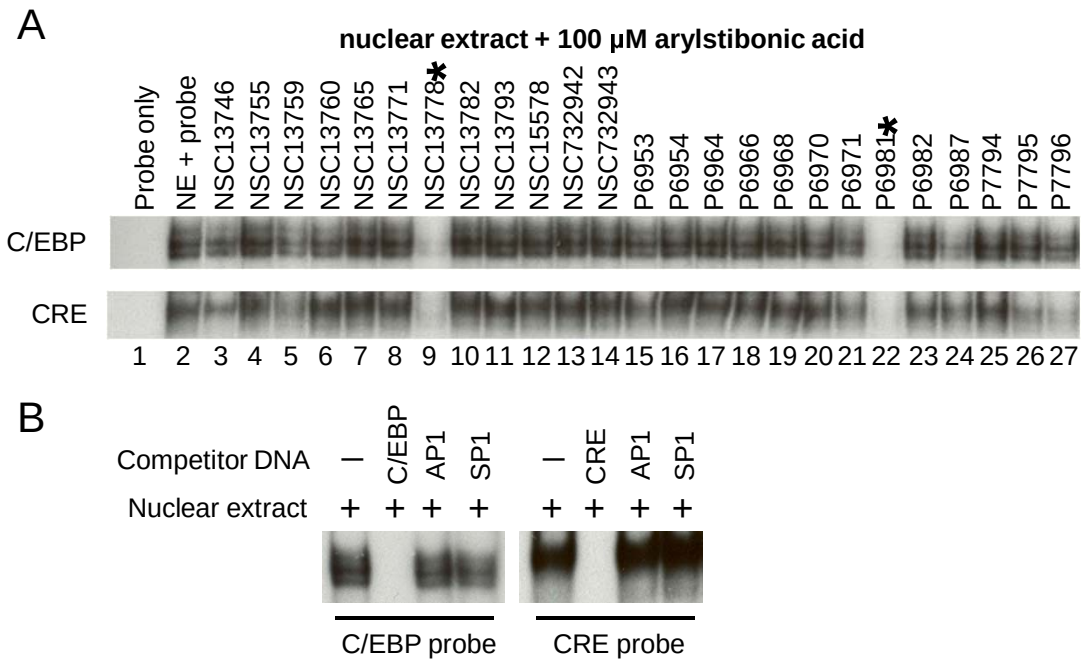

Molecular Pharmacology Fast Forward. Published on July 31, 2012 as DOI: 10.1124/mol.112.080820
This article has not been copyedited and formatted. The final version may differ from this version.

Fig. 7

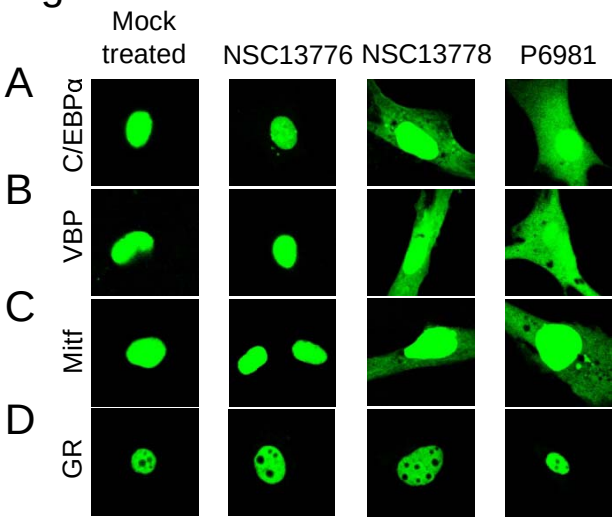

Molecular Pharmacology Fast Forward. Published on July 31, 2012 as DOI: 10.1124/mol.112.080820
This article has not been copyedited and formatted. The final version may differ from this version.

Fig. 8

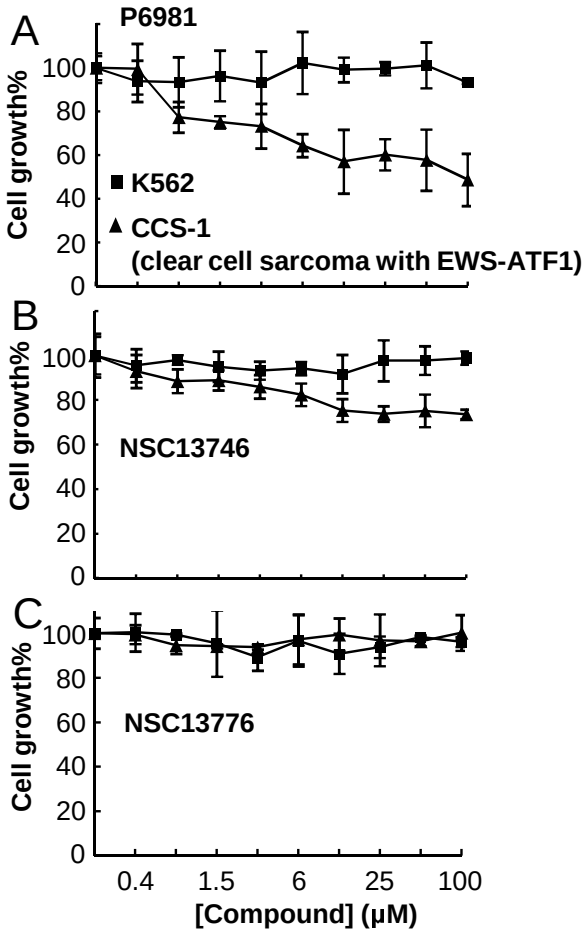

Molecular Pharmacology Fast Forward. Published on July 31, 2012 as DOI: 10.1124/mol.112.080820
This article has not been copyedited and formatted. The final version may differ from this version.

Fig. 9